Catalysis Today 171 (2011) 36–42

Contents lists available at ScienceDirect

Catalysis Today

journal homepage: www.elsevier.com/locate/cattod

Simultaneous optimization of methane conversion and aromatic yields by catalytic activation with ethane over Zn-ZSM-11 zeolite: The influence of the Zn-loading factor

Oscar A. Anunziata*, Jorgelina Cussa, Andrea R. Beltramone

Grupo Fisicoquímica de Nuevos Materiales, CITeQ, Facultad Regional Córdoba, Universidad Tecnológica Nacional, 5016 Córdoba, Argentina

ARTICLE INFO

Article history:
Received 30 October 2010
Received in revised form 28 April 2011
Accepted 28 April 2011
Available online 12 June 2011

Keywords:
Experiment design
Response Surface
Two responses
Methane activation
Zn-loading factor

ABSTRACT

Experiment design-response surface methodology (RSM) is used in this work to model and optimize two responses in the process of activation of methane (C1) using ethane (C2) as co-reactant into higher hydrocarbons, over Zn-containing zeolite catalysts. The application of this methodology provides insights into a more comprehensive understanding of the influence attributed to from the different factors. In this study we analyze the influence of the C1 molar fraction (C1/C1 + C2), the reaction temperature and the Zn-loading factors. The responses analyzed were as follows: Y1: C1 conversion (mol% C) and Y2: aromatic hydrocarbon yields (mol% C). The response surfaces were obtained with the Box–Behnken Design, finding the best combination between the reaction parameters that allowed optimizing the process. By applying the statistic methodology, the higher levels of the two objective functions, C1 conversion of 48.6 mol% C and aromatic yields of 47.2 mol% C, were obtained employing, a higher temperature, 0.2–0.4 molar fraction of C1 and the catalysts with a higher Zn^{2+} content.

1. Introduction

The natural gas (NG) constitutes a valuable, accessible and economical energy source which impacts significantly on the world energy balance, considered to be an alternative source of fuel and other petrochemical products. The activation and direct conversion of methane involve a promising approach for adopting natural gas resources, also posing a major challenge in the science of catalysis. In previous research, the aromatization of C1 using light paraffin as a co-reactant over Zn-ZSM-11 catalyst [1–3] was reported. C1 would be activated under non-oxidizing conditions by interaction with C2 and LPG. Particularly high levels of C1 conversion to Aromatic Hydrocarbons were obtained by interaction with C2 (molar fraction in the feed: C1/C1 + C2 = 0.4–0.8) over Zn-ZSM-11 (molar fraction $Zn^{2+}/Zn^{2+}H^{+}$ = 0.86) at 550 °C and a total pressure of 1 atm, with an aromatic hydrocarbon yield range of 10–40 mol% C1 [3]. Anunziata et al. [1] found that, in the activation of C1 with LPG, aromatic hydrocarbons were the main products in the whole range of C1 molar fractions (0.4–0.85), reaching higher levels of C1 conversion (10–45%). Anunziata [4] reported the optimizations of methane conversion with ethane over Zn/HZSM-11 zeolite as the only objective function. Anunziata and Cussa [5] analyzed the influence of four variables: TOS, GHSV-C2 and XC1 applying the statistic methodology, via which the process was optimized.

From the catalytic point of view, and according to our previous results of C1 activation with C2 [2–5], the reaction mechanism seems to be Rydeal-type. Ethane is adsorbed onto the catalyst surface generating active ad-species, which are impacted from the gas phase by C1. The Zn-species incorporated into the catalyst are active because of their lower LUMO energy (low unoccupied molecular orbital), acting as new and strong Lewis acid sites, and allowing the chemisorption of active C2 ad-species by the direct abstraction of a hydride, producing a carbenium-like surface species through electron donor–acceptor adduct (EDA) formation. These species then react in order to produce intermediates (such as C3 and C4) and more reactive olefins (C2, C4), and then isoparaffin (i-C4). The carbenium ad-species formed interact with C1 producing their transformation to naphthenics and aromatics. It should be noted that the presence of strong Lewis sites (SLS) on the Zn-ZSM-11 catalyst prevents the hydrogenation of intermediate alkenes, which would be efficiently introduced into the complex mechanism

* Corresponding author at: Centre of Research and Chemistry Technology, Grupo Fisicoquímica de Nuevos Materiales, CITeQ, Facultad Regional Córdoba, Universidad Tecnológica Nacional, Cruz Roja Argentina Y mAestro Lopez, 5016 Córdoba, Argentina. Tel.: +54 351 4690585; fax: +54 351 4690585.
E-mail address: oanunziata@scdt.frc.utn.edu.ar (O.A. Anunziata).

0920-5861/$ – see front matter © 2011 Elsevier B.V. All rights reserved.
doi:10.1016/j.cattod.2011.04.040

Table 1
Chemical composition of the catalysts employing different methods.

Catalyst	Chemical composition						
	Si/Al[a]			Al/Zn[a]			Zn^{2+} (mol/uc)
	ICPE	EDX	XPS	ICPE	EDX	XPS	ICPE
H-ZSM-11 (a)	16.9	18.0	93.0	–	–	–	–
Zn/HZSM-11 (b)	17.0	18.2	93.5	10.0	11.0	98.7	0.54
Zn/HZSM-11 (c)	17.0	18.2	93.5	3.7	5.0	97.0	1.33
Zn/HZSM-11 (d)	17.2	18.5	94.0	2.5	2.8	93.0	2.11

[a] Molar ratio.

of polymerization, cyclization, dehydrogenation and aromatization. The selective aromatics formed are benzene, toluene and xylenes.

The statistical experiment design implies the process of planning an experiment to obtain appropriate data subject to the analysis of statistical methods, to arrive at valid and accurate conclusions. The objective of all experiments includes the description of the responses to treatment factors. The origin of the experiment design can be traced to the twenties and attributed to the mathematician Fisher [6]. Specifically, the response surface design is classified as a simultaneous method, implemented in the stage of optimization. Its application allows selecting the optimum level combinations to obtain the best possible response for a specific condition [7]. The experimental design has been recently applied to the optimization of several processes [8–12]. In engineering, process modeling and optimization are especially significant for meeting the strictest quality requirements in a globally competitive market [13]. The objective is to select the levels of independent variables that optimize simultaneously all the responses. Experiment design-response surface methodology (RSM) is used in this work to model and optimize two responses in the process of methane (C1) activation using ethane (C2) as a co-reactant in higher hydrocarbons, over Zn-containing zeolites. In this study a Box–Behnken design was applied in order to analyze the influence of the following factors: Zn-loading, XC1 (C1/C1 + C2, C1 molar fraction) and reaction temperature. The data of total conversion and aromatic yields were calculated on C number basis mol% C, i.e., yield in mol% C of HC*i* = wt. (g) HC*i* × N of C atoms in the molecular formula × 100/molecular weight of HC*i*. The response analyses were: Y1: C1 conversion (mol% C) and Y2: aromatic hydrocarbon yields (mol% C). The response surfaces were obtained with the Box–Behnken Design, finding the best combination between the reaction parameters which would allow optimizing the process. By applying the statistic methodology with the better catalyst, the higher levels of the operation conditions of the two objective functions were as follows: C1 conversion of 48.6 mol% C and aromatic yields of 47.2 mol%. Box–Behnken design was developed with different levels of the factors, in which its influence on the C1 conversion to aromatic hydrocarbons was determined in order to obtain response surfaces.

2. Materials and methods

2.1. Synthesis

ZSM-11 zeolite with a Si/Al ratio of (17) was obtained by sol-gel technique using an ethanol–acetone–tetrabutylammonium hydroxide (TPAOH) mixture as a template [14]. The samples were prepared with the following reactants: tetraethylorthosilicate as the source of silicon; sodium aluminate as the source of aluminum and the template mixture. The synthesis procedure is described in terms of the following steps:

Table 2
Physical–chemical characterization results of the catalysts.

Catalyst	Area, BET (m^2/g)	Crystal size, SEM (μm)	Crystallinity, XRD (%)
H-ZSM-11 (a)	412	$1.3 \times 1.2 \times 2.5$	100
Zn/HZSM-11 (b)	405	$1.25 \times 1.2 \times 2.4$	>99.9
Zn/HZSM-11 (c)	400	$1.2 \times 1.2 \times 2.4$	>99.5
Zn/HZSM-11 (d)	398	$1.2 \times 1.2 \times 2.3$	>99.5

Step a: TEOS was hydrolyzed with HCl for 1 h and Al source in water was added to the resulting solution at 0 °C. The clear solution obtained was stirred for 20 min.
Step b: The final solution of step (a) was converted into a solid xerogel by addition of the corresponding templates at room temperature. The xerogel obtained was dried overnight at 110 °C.
Step c: The xerogel obtained in step (b) was impregnated with the adequate template solution by wetness impregnation method. The impregnated SiO_2/Al_2O_3 was charged in a Teflon-lined autoclave and crystallized at 150–160 °C for 20–36 h.

The molar composition of the gel-material previous to the crystallization was:

$$[(TBA)_2O]a\,[Acetone]a_1\,[Ethanol]a_2\,[Na_2O]b\,[Al_2O_3]x\,[SiO_2]y\,[H_2O]z$$

$a = 0.6\text{–}1 \times 10^{-3}$ mol; $a_1 = 0.8\text{–}1 \times 10^{-5}$ mol;

$a_2 = 0.3\text{–}0.5 \times 10^{-5}$ mol; $b = 4\text{–}5 \times 10^{-3}$ mol;

$x = 2.3\text{–}2.5 \times 10^{-3}$ mol; $y = 4.4\text{–}4.6 \times 10^{-2}$ mol;

$z = 1.5\text{–}3 \times 10^{-4}$ mol

The final product was then washed with distilled water, dried at 110 °C and heated for 12 h under nitrogen flow of 10 ml/min and 2 °C/min from 100 °C to 500 °C, which allowed us to avoid the migration of Al to extra-framework. Afterwards, the samples were calcined in air at 500 °C for 8 h and Na-ZSM-11 powder was obtained.

The proton forms of the catalysts were prepared by ion exchange of Na-ZSM-11 powder with 1 M ammonium chloride at 80 °C for 40 h followed by 16 h calcination under nitrogen and 10 h under air. Zn/HZSM-11 samples with different zinc contents were prepared by ion-exchange of NH_4^+-zeolite with zinc nitrate solutions (0.05 M, 80 °C for 4–30 h). The different Zn^{2+} molar fractions $\{Zn^{2+}/Zn^{2+} + H^+\}$ samples used in this study were denoted as follows: (a) H-ZSM-11; (b) Zn/HZSM-11{0.24}; (c) Zn/HZSM-11{0.55}; (d) Zn/HZSM-11{0.86} (Tables 1 and 2).

2.2. Characterization

The chemical composition of the samples, Si/Al; Al/Zn molar ratio and Zn by cell unit on the final catalysts, was calculated first, using an atomic absorption spectrometer (ICP). The catalysts were also characterized by powder XRD patterns using a synchrotron radiation source in the Laboratorio Nacional do Luz Synchrotron, LNLS, Campinas, SP, Brazil. The reference XRD patterns of other possible phases in the materials were taken from International Center for Diffraction Data. BET surface area determinations were carried out with ASAP 2010 equipment. Infrared measurements were performed on a JASCO 5300 FTIR spectrometer. For structure characterization, the samples were mixed with KBr and pressed to form a wafer. For their acidic properties, the samples were pressed into self supporting wafers (8–10 mg/cm^2). Pyridine (3 Torr) was adsorbed at room temperature for at least 2 h, and desorbed for 2 h at 250, 350 and 400 °C at 10^{-4} Torr.

The number of Brönsted and Lewis sites was determined using the literature on the integrated molar extinction coefficients [15], showing no dependence of the integrated coefficients on the catalyst or strength. The crystal size and the shape of the samples were determined using a scanning electron microscopy, PHILIPS SEM 501 B, equipped with an EDX probe for the semi-quantitative direct analysis of the elements. A drop of the sample solution was placed onto a glass wafer, dried at room temperature and sputtered with gold. X-ray photoelectron spectroscopy was performed on a VG ESCALAB MK2 spectrometer equipped with a hemispherical electron analyzer and an Al Kα X-ray source; thus, XPS analyses were carried out to further understand the nature and distribution of Zn species over ZSM-11 zeolites, showing the BE of Zn 2p3/2 core level at 1021 eV and the Zn 2p1/2 core level at 1044 eV, and indicating that the Zn^{2+} species are present over ZSM-11 zeolites [16–18].

2.3. Reaction conditions

The catalytic reactions of C1 + C2 were carried out in a fixed-bed continuous flow quartz reactor, with a 10 mm inner diameter and a 20 cm length, at a different reaction temperature over Zn-ZSM-11 catalyst. The catalyst diluted in crushed quartz (100 mg catalyst/700 mg quartz) was added to the reactor to minimize homogeneous reactions. In order to ensure be sure that quartz was not active in the reaction, a reaction blank was performed and the conversion was zero. The catalyst particles were held on quartz wool plug, placed in the middle of the reactor. It was first degassed by blowing with N_2 at 600 °C for 2 h. The bed temperature was then adjusted to the required values with temperature controller. The furnace was a close-fitting, well-insulated stainless steel block, heated externally with a temperature heater. This construction allows for effective heat transfer to the reactor wall, and provides isothermal operation of the reaction zone. This reactor operated at atmospheric pressure, on-line, through automatic sampling, with a gas chromatograph equipped with a FID detector. Products were withdrawn periodically from the outlet of the reactor and analyzed using a 2.2 m Porapak Q column. The delivery tubes were all heated to 210 °C at the exit of the reactor, to avoid liquid condensation in the pipework [4]. Replicate runs give a standard deviation in the methane and ethane conversion of 0.4–0.2 mol% C, respectively. The following reactants were used as feed: high purity methane (>99.97%) and ethane (>99.997%) supplied by AGA. The C1/(C1 + C2) molar fractions were selected as a function of the C1 conversion. Above 0.8, the C1 was not activated, around 0.4, the C1 conversion was high but the highest conversion was about 0.8. The GHSV of C2 was chosen according to the previous reports [2,3], where C2 alone generated reactive ad-species (ethyl carbenium ad-species, ethene, etc., and lower aromatic products), which could interact with C1 to activate it. Thus, the C2 GHSV was 810 ml/g h. The values of the TOS were taken up, as the conversion of C1 reached a 5% minimum conversion and the deactivation of the catalyst was not observed. Hence, 20 min was selected as the time-on-stream.

3. Results and discussions

Tables 1 and 2 show physical-chemical results obtained applying different characterization methods of the samples employed in this work.

According to the surface analysis, with diverse depth information, i.e., XPS 5–8 nm, EDX 1–5 μm and ICPE, and bulk composition, if we analyze Table 1, with SEM data of crystal size lower than 4 μm (Table 2), we can infer from the samples obtained by ion exchange that:

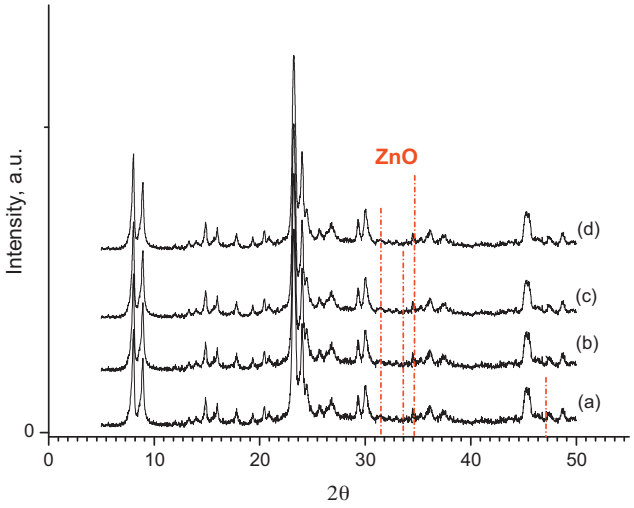

Fig. 1. XRD pattern of the samples indicating the presence of ZnO at 30–40 2θ for ZnH/ZSM-11 (b); (c and d) HZSM-11 (sample shown for comparison).

(a) For H- and Zn-samples, the Al incorporated within the channel of the zeolite (Si/Al = 17–19, by ICPE and EDX) was higher than that on the outer surface (Si/Al = 93–94 by XPS) in H and Zn-zeolites.
(b) As the zinc was incorporated as a counter ion, two Al were required in a nearly geometrical neighborhood to interact with one Zn^{2+}; if the Al content on the outer surface (depth 5–8 nm by XPS) was especially low, the Zn content was also low (Al/Zn = 93–98 by XPS) in Zn-containing zeolite but 2.7–11 from ICPE and EDX.
(c) ICPE and EDX (bulk results according to the crystal size by SEM) therefore resemble each other, but differ significantly from XPS data, which allows suggesting that more Zn^{2+} species can be found within the channel of the zeolite than on the outer surface.

The values provided in Table 1 show that for Zn/HZSM-11 (d): Si/Al by EDX = 18.5; by XPS = 94. Al/Zn by EDX = 2.8; by XPS = 93.
(d) Therefore Si/Zn by EDX = 97.2; by XPS = 8.7. The EDX data differ notably from XPS results.
(e) In each sample we can see that Si/Al and Al/Zn ratios by XPS are very similar, indicating that while Al or Zn increases, their concentration within the zeolite crystal also increases as well.

The samples used in XRD and FTIR studies were Zn/HZSM-11 (a–c) with 0.54, 1.33 and 2.11 mol of Zn^{2+}/unit cell, respectively, and HZSM-11 for comparing the active sites as the zinc loading increased.

3.1. XRD studies

X-ray diffraction analysis with Synchrotron radiation confirms the tetragonal symmetry of the ZSM-11 materials synthesized, showing the following lattice parameters: Space group: $I-4m^2$; a = 20.067 Å; b = 20.067 Å; c = 13.411 Å; UC volume = 5361.95 $Å^3$, free from other phases. The experimental data obtained by least-squares fit to interplanar spacing of selected reflections in the X-ray diffraction pattern [21] display satisfactory accuracy, despite being somewhat limited by the convolution among diffraction lines in the X-ray pattern of MEL-type structures. Likewise, we studied the possibility of detecting other phases such as zinc oxide, especially in the samples with higher Zn content. Fig. 1 shows the XRD patterns of samples (g–j). For ZnO, no presence of ZnO species as an isolated cluster can be found in view of the literature data (PDF: 36-1451 and CAS N; 1314-13-2). Moreover, taking account of the

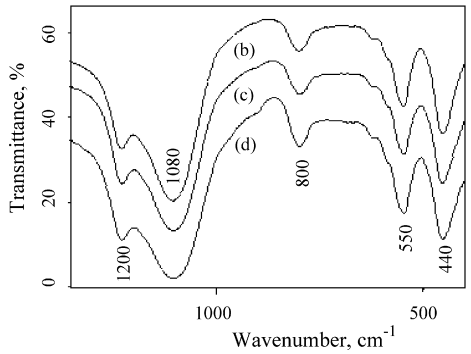

Fig. 2. FTIR (fingerprint zone) of Zn/HZSM-11 zeolites, samples (b–d).

results reported by McMurdie [19], which show four characteristic signals for ZnO with relative intensities, Fig. 1 exhibits 57, 44, 100 and 23 at: 31.77, 34.42, 36.25 and 47.54 2θ, respectively (bar line).

3.2. IR spectroscopic studies

Fig. 2 depicts the IR spectra of the Zn-containing zeolites in the region of 1400–400 cm^{-1}. As seen, all the samples show good crystallinity, taking into account the intensity ratio at 550/450 cm^{-1}, characteristic of MEL-phase.

Fig. 3 shows the spectra of: (a) H-ZSM-11 (17), (b–d) Zn/HZSM-11 from lower to higher Zn content respectively, in the range 3900–3500 cm^{-1}. All the samples exhibited an IR band at 3740 cm^{-1}, indicating the presence of very low terminal Si–OH, as the template (tetrabutylammonium hydroxide) and co-template (using ethanol–acetone) mixture inhibits Si–OH formation. The IR band at 3610 cm^{-1} can be assigned to Bronsted acid sites [Si_3(OH)Al], found in all samples except in (d), with very low Bronsted sites, indicating their exchange for Zn^{2+}.

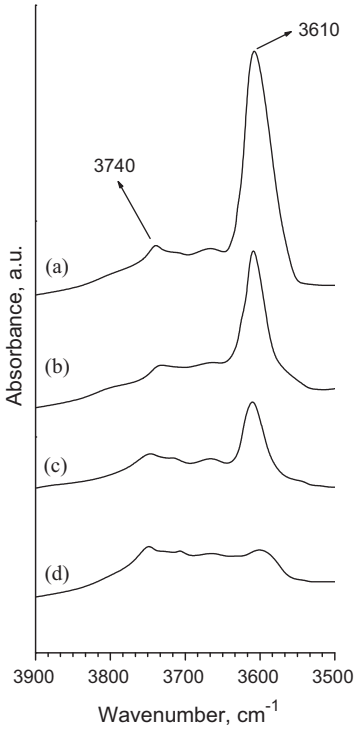

Fig. 3. FTIR in O–H stretching of: (a) H-ZSM-11 (17); Zn/HZSM-11 samples (b–d).

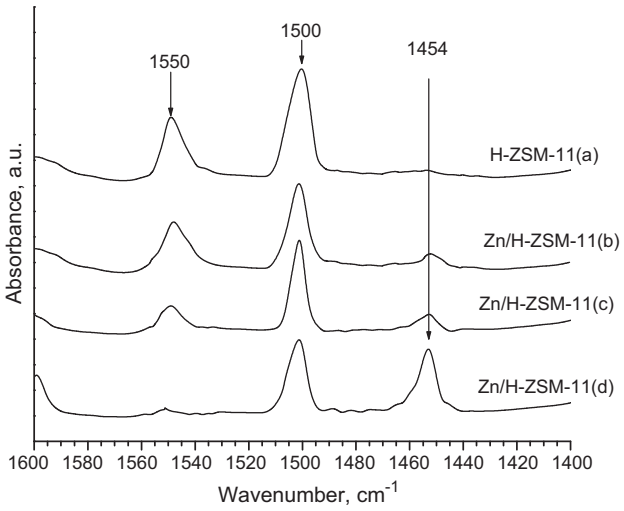

Fig. 4. FTIR spectra for chemisorbed pyridine after adsorption at room temperature and 3 Torr and outgassing the samples at 400 °C at 10^{-4} Torr.

Fig. 4 shows the IR spectra for chemisorbed pyridine after adsorption at room temperature and 3 Torr. After further outgassing the samples at 400 °C at 10^{-4} Torr, this study allowed us to determine the concentration of Bronsted-acid and Lewis-acid sites. The concentration of pyridine interacting with Bronsted acid sites PyH^+ was calculated from the maximum intensity of the absorption at 1545 cm^{-1}. The absorption band at 1450–1460 cm^{-1} indicates the electron-donor–acceptor adduct EDA of pyridine-Lewis sites in zeolites.

The results suggest that in the zeolites with Zn^{2+} species, a higher proportion of Lewis sites are present in the following samples order: d > c > b ⋙ a. However, while the number of OH sites decreases when Zn loading is higher (sample d with Zn molar fraction 0.86), a few –OH Bronsted appears, as their interaction with two neighbor-exchanged sites (Zn^{2+}-containing zeolite-type ZSM-11) [20] is more feasible. On the other hand, the sample without Zn (proton expression of ZSM-11, sample a) shows very few Lewis sites in agreement with the lower Si–OH sites shown in Fig. 3, and the resulting decrease in sp^2 aluminum hybridization.

The Zn/HZSM-11 samples showed in Table 3 (b–d with 0.54, 1.33 and 2.11 mol of Zn^{2+}/unit cell respectively), were obtained by ion exchange, except the sample (e) which was prepared by incipient wetness impregnation of HZSM-11 and not employed in the present optimization study. It is evident that the sample (e), shows a very low Lewis sites, due to the main Zn species were like as Zn-oxide, whereas the other Zn-containing zeolite, obtained by ion exchange, the weak, medium and specially the strong Lewis sites increases as the Zn content increases, supporting the idea that the zinc was incorporated as Zn^{2+}.

Table 3
FTIR quantification of acidic sites using pyridine (Py), at different desorption temperatures and 10^{-4} Torr.

Catalyst	FTIR[a], retained Py (μmol/g)					
	300–200 °C		400–300 °C		>400 °C	
	WBS	WLS	MBS	MLS	SBS	SLS
H-ZSM-11 (a)	93	7	79	5	74	1
Zn/H-ZSM-11 (b)	47	76	71	56	49	65
Zn/H-ZSM-11 (c)	41	95	65	74	41	158
Zn/H-ZSM-11 (d)	24	146	51	108	22	243
Zn/H-ZSM-11 (e)[b]	56	21	75	15	60	55

[a] BS: Brönsted sites; LS: Lewis sites; W: weak; M: medium; S: strong.
[b] Prepared by incipient wetness impregnation of HZSM-11.

Table 4
Coded and decoded levels of the factors.

Coded levels	Zn[a]	XC1	Reaction temperature (°C)
(−1)	0.24	0.2	520
(+1)	0.86	0.6	580
(0)	0.55	0.4	550

[a] $Zn^{2+}/Zn^{2+}H^{+}$.

Table 5
The Box–Behnken design, showing the responses and the coded and decoded levels of the factors; some relevant data.

Factors Decoded			Coded			Responses	
Zn	XC1	React. Temp.	X_1	X_2	X_3	C1 Conv.	Aromatic hydrocarbons
0.55	0.6	580	0.0	1.0	1.0	28.00	22.5
0.86	0.6	550	1.0	1.0	0.0	26.67	30.2
0.55	0.4	550	0.0	0.0	0.0	35.00	31.0
0.24	0.4	520	−1.0	0.0	−1.0	18.00	17.0
0.55	0.6	520	0.0	1.0	−1.0	15.00	14.0
0.55	0.4	550	0.0	0.0	0.0	26.67	30.2
0.55	0.4	550	0.0	0.0	0.0	27.01	29.4
0.86	0.4	580	1.0	0.0	1.0	50.40	33.0

Table 6
Analysis of variance to C1 conversion (ANOVA).

Source of variation	Sum of squares	Df	Mean square	*F*-Ratio	*p*-Value
X_1: (Zn)	397.056	1	397.056	9.77	0.0141
X_2: (XC1)	138.112	1	138.112	3.40	0.1024
X_3: (Temp.)	285.605	1	285.605	7.03	0.0292
X_1X_2	53.436	1	53.4361	1.32	0.2846
X_1X_3	141.61	1	141.61	3.49	0.0989
X_2X_3	37.21	1	37.21	0.92	0.3666
Total error	324.997	8	40.624		
Total (exp.)	1378.03	14			

4. Design

Continuing the analysis performed by Anunziata and Cussa [5], where significant factors such as XC1, reaction temperature and TOS–reaction temperature interaction, in this research we introduce the influence of a highly important variable: the Zn-loading factor. Three catalysts differing in Zn content were examined (samples b–d). A Box–Behnken design was applied and the variables studied were: Zn-loading, molar fraction of C1/C1 + C2 and reaction temperature. The natural variables (factors) were codified for a better data treatment. This is a simple linear transformation of the original measurement scale for a factor; thus, the high value becomes +1 and the low value becomes −1. Box–Behnken design has 15 experiments; the runs were randomly carried out and the data obtained were analyzed at the 95.0% confidence level. Table 4 shows the factor levels employed. The zinc loading, $Zn^{2+}/Zn^{2+}H^{+}$ factor was denoted as Zn. The TOS was 20 min and the GHVS-C2 was 810 ml/g h.

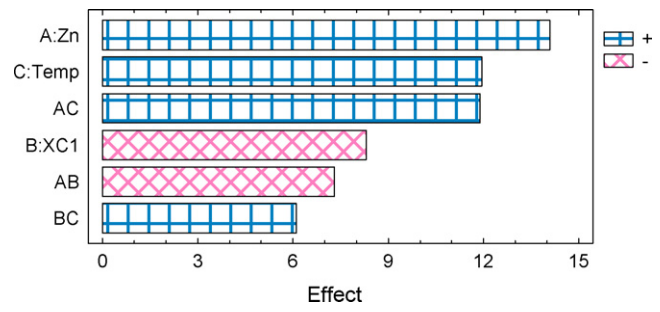

Fig. 5. Pareto of effects on C1 conversion.

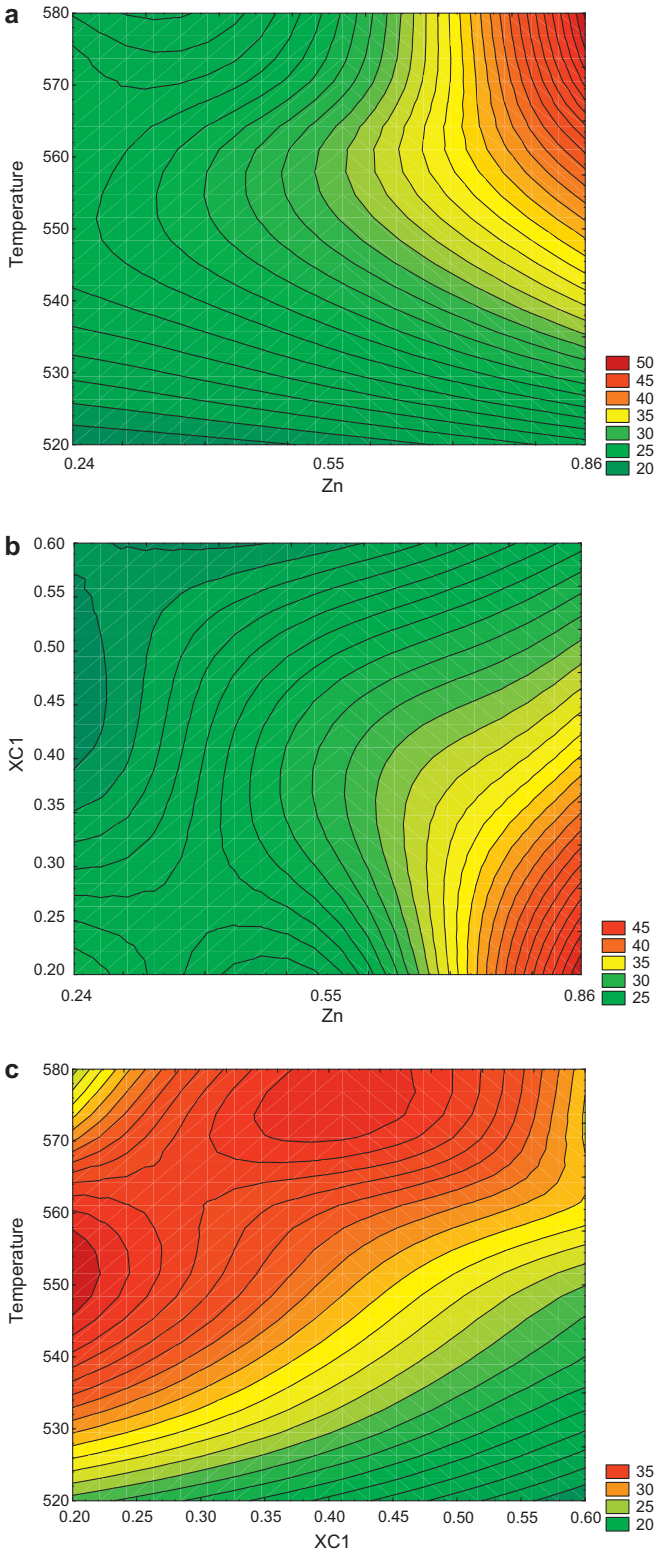

Fig. 6. Response surface fitted for the design. C1 conversion as a function of: (a) Zn content and reaction temperature; (b) Zn content and XC1; (c) XC1 and reaction temperature.

Table 7
Analysis of variance to aromatic hydrocarbon yield.

Source of variation	Sum of squares	Df	Mean square	*F*-Ratio	*p*-Value
X_1: (Zn)	210.125	1	210.125	5.48	0.0474
X_2: (XC1)	213.108	1	213.108	5.56	0.0462
X_3: (Temp.)	95.842	1	95.842	2.50	0.1526
X_1X_2	12.96	1	12.96	0.34	0.5771
X_1X_3	0.64	1	0.64	0.02	0.9004
X_2X_3	13.359	1	13.359	0.35	0.5714
Total error	306.88	8	38.3601		
Total (exp.)	852.92	14			

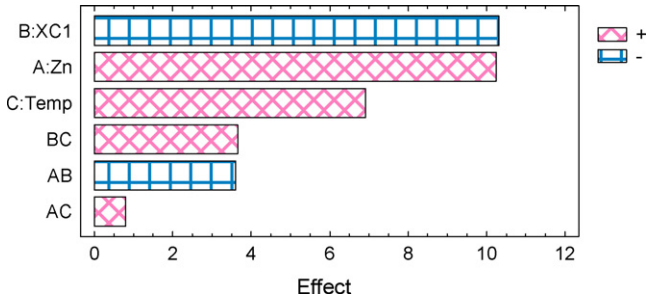

Fig. 7. Pareto of effects on aromatic hydrocarbon yields.

4.1. Experimental design-response surface

In the response surface methodology (RSM), factorial designs are carried out, and the results are adjusted using mathematical models. These stages are known as displacement stage and design, respectively; they are repeated several times, screening the response surface obtained in the direction of the region of the best optimum point.

In this study, a Box–Behnken design was applied. Table 5 shows some relevant data of the design using Statgraphics and Statistica software.

4.2. Response: C1 conversion

For each effect, the variance analysis (ANOVA) [21] partitions the variability of the response into separate pieces. ANOVA then tests the statistical significance of each effect by comparing the mean square against an estimate of the experimental error (Table 6).

The results obtained by the ANOVA test show, in this case, that two effects are significantly different from zero at the 95.0% confidence level (these *p*-values were highlighted as bold values). Such factors are Zn and Temperature. One effect is markedly different from zero at the 90.0% confidence level, i.e., Zn–Temperature interaction. The *R*-squared statistic [22] indicates that the model accounts for 76.41% of the variability found in C1 conversion. Here, this value indicates that the model explains 76% of the total variations.

According to the Pareto seen in Fig. 5, the following can be underlined: the parameters that produce a more pronounced effect on the C1 conversion are Zn, temperature and Zn–temperature interaction. The positive sign in the effect of the factors suggests an increase in the response of the change from the lower to the higher level of the factor. The negative sign implies a decrease in the response of the change from the lower to the higher level of the factor.

Table 8
C1 conversion and aromatic hydrocarbon yields in the optimal conditions.

XC1	Temp. (°C)	$Zn^{2+}/Zn^{2+} + H^+$ molar fraction	C1 Conv. (mol% C)	Aromatic hydrocarbon (mol% C)
0.2	550	0.86	48.6	47.2
0.2	580	0.86	50.5	44.1
0.4	550	0.86	50.0	37.0
0.4	580	0.86	50.4	33.0

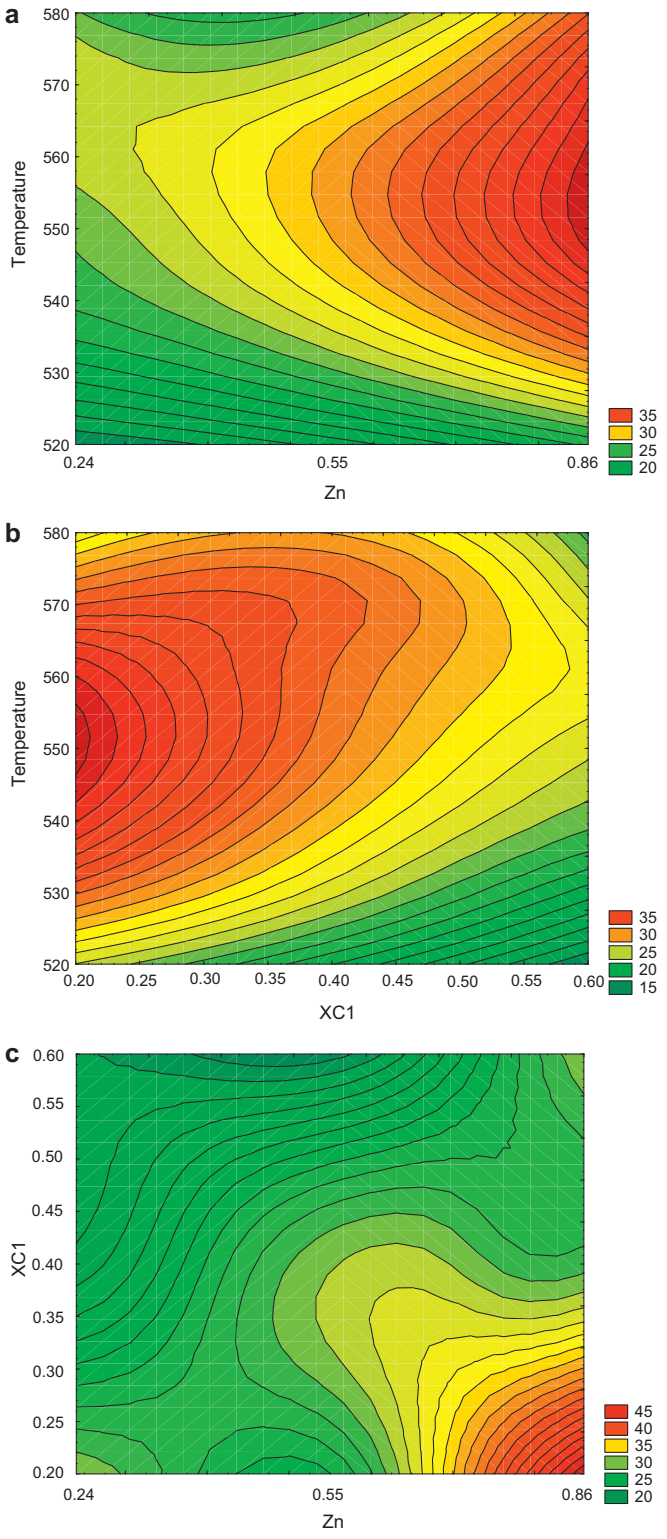

Fig. 8. Response surface fitted for the design. Aromatic hydrocarbon yield as a function of: (a) Zn and temperature; (b) Zn and XC1; (c) XC1 and temperature.

The model equation for the response surfaces fitted to the experimental data points is represented in coded units as follows:

$$\text{C1 conversion} = 27.7773 + 7.045 \times \text{Zn} - 4.155 \times \text{XC1} + 5.975 \times \text{Temp.} - 3.655 \times \text{Zn} \times \text{XC1} + 5.95 \times \text{Zn} \times \text{Temp.} + 3.05 \times \text{XC1} \times \text{Temp.} \quad (1)$$

The contours of estimated response surface products of the design are shown in Fig. 6.

4.3. Response: aromatic hydrocarbon yields

The results obtained by the ANOVA test show, in this case, that two effects significantly differ from zero at the 95.0% confidence level (Table 7). These factors are Zn and XC1. The *R*-squared statistic [21] indicates that the model accounts for 64.02% of the variability in the aromatic hydrocarbon yield. Here, the value evidences that the model explains 64% of the total variation.

According to the Pareto referred to in Fig. 7, the following aspect can be underlined: the fact that parameters producing the more noticeable effect on aromatic hydrocarbon yields are XC1 and Zn.

The model equation for the response surfaces fitted to the experimental data points is as follows:

$$\text{Aromatic hydrocarbon yields} = 26.9527 + 5.125 \times \text{Zn} - 5.16125 \times \text{XC1} + 3.46125 \times \text{Temp.} - 1.8 \times \text{Zn} \times \text{XC1} + 0.4 \times \text{Zn} \times \text{Temp.} + 1.8275 \times \text{XC1} \times \text{Temp.} \quad (2)$$

The contours of estimated response surface products of the design are shown in Fig. 8.

4.4. Optimization

The statistic methodology followed in this work, and considering Eqs. (1) and (2), the data and the response surfaces obtained allow suggesting the better operation conditions for this reaction in order to optimize the two responses (C1 conversion and aromatic hydrocarbon yield).

We suggest the better operation conditions as follows: XC1: 0.2–0.4; React. Temp.: 550–580 °C and $Zn^{2+}/Zn^{2+}H^{+} = 0.86$. To corroborate this, several reactions were performed in the optimal conditions (Table 8).

The results found in Table 8 show the optimal values of the reaction conditions, on the basis of statistic analyses.

5. Conclusions

An experimental design was carried out in order to optimize C1 conversion and aromatic hydrocarbon yields. The statistic model applied in this work has allowed us to optimize simultaneously two responses. Following the statistic methodology, the best operation conditions can be found. The highest C1 conversion (mol% C) and higher aromatic yields were achieved working in these conditions. Similarly, the statistic methodology indicates that Zn content, reaction temperature and Zn content reaction temperature interaction display the major effects on C1 conversion; Zn and XC1 show the more significant effects on aromatic hydrocarbon yields. Thus, we arrive at a higher C1 conversion (50 mol% C) and higher aromatic yield (47 mol% C). It is interesting to note that we have drawn these conclusions considering the influence of the separate variables and their main interaction. The presence of a higher amount of strong Lewis sites on the catalyst (with higher $Zn^{2+}/Zn^{2+}H^{+}$ molar fraction) inhibits the hydrogenation of intermediate alkenes, which would be efficiently introduced into polymerization, cyclization, and dehydrogenation and aromatization complex mechanism. The statistic model applied to this research has allowed us to interpret the overall process, considering the multivariate parameters. Applying the statistic methodology, the best operation conditions were obtained. High C1 conversion (48.6 mol% C) and aromatic hydrocarbon yields (47.2 mol%) were achieved under these conditions, advancing the results recently reported, where only one objective function (C1 conversion) could be optimized [4].

References

[1] O.A. Anunziata, G.A. Eimer, L.B. Pierella, Catal. Lett. 58 (1999) 235–239.
[2] O.A. Anunziata, G.A. Eimer, L.B. Pierella, Appl. Catal. A: Gen. 190 (2000) 169–176.
[3] L.B. Pierella, G.A. Eimer, O.A. Anunziata, Stud. Surf. Sci. Catal. Nat. Gas Conv. V 119 (1998) 235–240.
[4] O.A. Anunziata, J. Cussa, Chem. Eng. J. 138 (2008) 510–516.
[5] O.A. Anunziata, J. Cussa, Open Process Chem J. 3 (2010) 7–16.
[6] R.A. Fisher, The Design of Experiments, 2nd ed., Oliver and Boyd, Edinburgh, 1937.
[7] D.C. Montgomery, Design and Analysis of Experiments, John Wiley & Sons, Inc., New York, 1991.
[8] S. Ferreira-Dias, A.C. Correia, F.O. Baptista, M.M.R. da Fonseca, J. Mol. Catal. B: Enzym. 11 (2001) 699–711.
[9] G. Øye, J. SjÖblom, M. StÖcker, Microporous Mesoporous Mater. 34 (2000) 291–299.
[10] J. Guervenou, P. Giamarchi, C. Coulouarn, M. Guerda, C. le Lez, T. Oboyet, Chemom. Intell. Lab. Syst. 63 (2002) 81–89.
[11] O.A. Anunziata, A.R. Beltramone, J. Cussa, Appl. Catal. A: Gen. 270 (2004) 77–85.
[12] G. Du, Y. Yang, W. Qiu, S. Lim, L. Pfefferle, G.L. Haller, Appl. Catal. A: Gen. 313 (2006) 1–13.
[13] M. Sen, H.S. Shan, Robotics and Computer-Integrated Manufacturing, 2007, p. 2317.
[14] O.A. Anunziata, L.B. Pierella, G. Marino, Appl. Catal. 165 (1997) 35–49.
[15] C.A. Emeis, J. Catal. 141 (1993) 347.
[16] Z. Deng, M. Chen, G. Gu, L. Wu, J. Phys. Chem. B 112 (2008) 16–22.
[17] N.S. Ramgir, D.J. Late, A.B. Bhise, M.A. More, I.S. Mulla, D.S. Joag, K. Vijayamohanan, J. Phys. Chem. B 110 (2006) 18236–18242.
[18] E.V. Ramos-Fernandez, A.F.P. Ferreira, A. Sepulveda-Escribano, F. Kapteijn, F. Rodriguez-Reinoso, J. Catal. 258 (2008) 52–60.
[19] H. McMurdie, Powder Diffr. 1 (1986) 40.
[20] O.A. Anunziata, G. Gonzalez Mercado, Chem. Commun. 5 (8) (2004) 401–405.
[21] R.O. Kuehl, Design of Experiments, 2nd ed., Duxbury-Thomson Learning, Pacific Grove, 2000.
[22] G.E.P. Box, K.B. Wilson, J. R. Stat. Soc. Ser. B 13 (1951) 1–45.